

Numerical analysis of polarization gratings using the finite-difference time-domain method

Chulwoo Oh and Michael J. Escuti*

Department of Electrical and Computer Engineering, North Carolina State University, Raleigh, North Carolina 27695, USA

(Received 19 March 2007; published 12 October 2007)

We report the first full numerical analysis of polarization gratings (PGs), and study their most general properties and limits by using the finite-difference time-domain (FDTD) method. In this way, we avoid limiting assumptions on material properties or grating dimensions (e.g., no paraxial approximations) and provide a more complete understanding of PG diffraction behavior. We identify the fundamental delineation between diffraction regimes (thin versus thick) for anisotropic gratings and determine the conditions for $\approx 100\%$ diffraction efficiency in the framework of the coupled-wave ρ and Q parameters. Diffraction characteristics including the efficiency, spectral response, and polarization sensitivity are investigated for the two primary types of PGs with linear and circular birefringence. The angular response and finite-grating behavior (i.e., pixelation) are also examined. Comparisons with previous analytic approximations, where applicable, show good agreement.

DOI: 10.1103/PhysRevA.76.043815

PACS number(s): 42.40.Eq, 42.79.Dj, 42.25.Ja, 42.40.Lx

I. INTRODUCTION

Polarization gratings (PGs) [1–4] are generally described as periodic profiles of spatially varying optical anisotropy. Unlike conventional phase or amplitude gratings, they operate by locally modifying the polarization state of lightwaves passing through them. The most studied PG profiles are continuous and transparent, which we classify into two primary types based on their local anisotropy: “Circular PGs” [Fig. 1(a)] consisting of a spiraling, constant-magnitude, linear birefringence; and “linear PGs” [Fig. 1(b)] consisting of a varying-magnitude circular and linear birefringence. They manifest a unique combination of optical properties that can include 100% diffraction into a single order, diffracted orders with a fixed polarization state controlled by the PG profile, and efficiencies that are highly polarization sensitive. These make PGs useful for numerous applications in a variety of fields, including polarimeters, displays, polarizing beam splitters, beam steering, and polarization multiplexers [3,5,6].

The most popular means to create PGs is using polarization holography with anisotropic organic recording materials (especially azobenzene-containing polymers [7–9]), among other materials [10–12]. PGs also can be formed by sub-wavelength features [5,13]. Several related approaches use patterned surfaces to align a liquid crystal layer [14–16], which have recently been implemented experimentally with ideal optical properties [17–19]. The analysis here applies to all of the above.

In this work, we present an extensive numerical analysis of the optical properties of PGs using the finite-difference time-domain (FDTD) method [20]. While concise analytic expressions for the optical properties of PGs have been derived [1,4,7] using Jones calculus [21], these are limited by their assumptions to large grating periods, normal incidence, and infinite gratings. Furthermore, even the most unabridged coupled-wave analysis [2] is limited to slowly varying enve-

lopes, and has only been developed for pure volume holograms. No work adequately deals with the fundamental question of delineating the thin or thick grating regimes in anisotropic gratings. Therefore, we aim to investigate three issues: First and most prominently, we seek to understand PG behavior as the grating period becomes comparable to the wavelength; second, we predict the angular response and the behavior of a finite grating; third, we confirm the paraxial analytic expressions. We use the freely available software package WOLFSIM—*Wideband Optical FDTD Simulator*, developed at NCSU for periodic anisotropic media [22,23].

II. FDTD IMPLEMENTATION AND PG DEFINITION

Propagation of light waves in a source-free space is governed by Maxwell’s curl equations: $\nabla \times \mathbf{E} = -\partial \mathbf{B} / \partial t$ and $\nabla \times \mathbf{H} = \partial \mathbf{D} / \partial t$. The constitutive relations for anisotropic dielectric media are $\mathbf{D} = \epsilon_0 \tilde{\epsilon} \mathbf{E}$ and $\mathbf{B} = \mu_0 \tilde{\mu} \mathbf{H}$, where the tilde signifies a tensor and ϵ_0 and μ_0 are the permittivity and the permeability of free space, respectively. Here, we assume nonmagnetic media ($\tilde{\mu}$ is a unity matrix). FDTD simulations solve Maxwell’s equations within a computational grid space

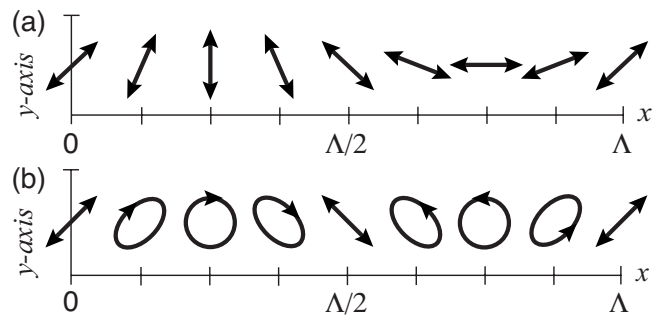


FIG. 1. Periodic anisotropy profiles for the two primary types of PGs studied here: (a) Circular PG and (b) linear PG. The direction or handednesses of the total local anisotropy are illustrated as arrows. (Λ is the effective optical grating period.)

*mjescuti@ncsu.edu

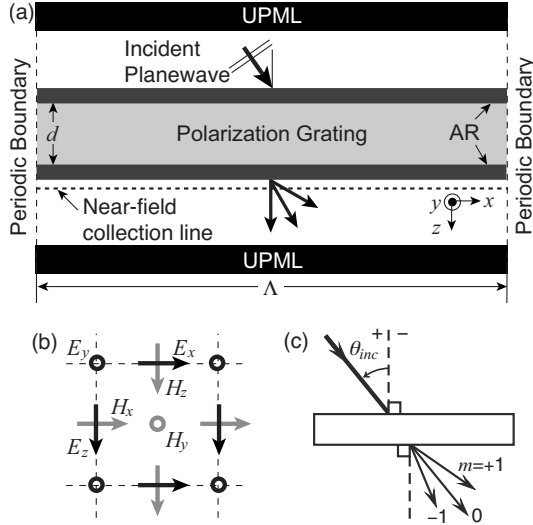


FIG. 2. Schematics of the 2D FDTD simulation space: (a) layout of simulation space (not drawn to scale); (b) field distribution on square-grid lattices; (c) diffraction order geometry and notation. Note that the x width is determined by the grating period Λ .

in the time domain, and have become one of the most powerful tools for electromagnetic propagation or scattering problems.

Our custom FDTD implementation (WOLFSIM) [22] incorporates a two-dimensional (2D) spatial grid containing media with an arbitrary three-dimensional, nondispersive permittivity tensor. Off-axis illumination, monochromatic and wide-band (Gaussian-pulse) sources, and periodic boundaries are explicitly incorporated.

We consider structures with 1D periodicity along the x axis. Figure 2 illustrates a 2D FDTD simulation space with offset, square-grid lattices for PG analysis [24]. The heart of the simulation is a modified split-field [25] method, adapted for arbitrary anisotropic media [22] with input illumination at a general angle of incidence. The boundaries in the x direction are terminated by Bloch periodic boundary conditions, while the boundaries in the z direction are terminated with uniaxial perfectly matched layers (UPML) [26]. A complete description of the details can be found in Ref. [22].

The permittivity tensor $\tilde{\epsilon}$ defines PG structures in the simulation space. A generic, in-plane, uniaxial anisotropy with gyration [27] can be written as

$$\tilde{\epsilon} = \begin{bmatrix} \epsilon_{xx} & \epsilon_{xy} & \epsilon_{xz} \\ \epsilon_{yx} & \epsilon_{yy} & \epsilon_{yz} \\ \epsilon_{zx} & \epsilon_{zy} & \epsilon_{zz} \end{bmatrix} = \mathbf{R}^{-1}(\phi) [\tilde{\epsilon}_{\text{lin}} + \tilde{\epsilon}_{\text{cir}}] \mathbf{R}(\phi), \quad (1)$$

where $\tilde{\epsilon}_{\text{lin}}$ and $\tilde{\epsilon}_{\text{cir}}$ are tensor elements corresponding to linear and circular anisotropy, respectively, as follows:

$$\tilde{\epsilon}_{\text{lin}} = \begin{bmatrix} n_{\text{ex}}^2 & 0 & 0 \\ 0 & n_{\text{or}}^2 & 0 \\ 0 & 0 & n_{\text{or}}^2 \end{bmatrix}, \quad (2a)$$

TABLE I. Material parameters for PGs studied here.

| | Circular PG | Linear PG |
|--------------------|--------------------------|---|
| $\phi(x)$ | $x\pi/\Lambda + \pi/4$ | $\pi/4$ |
| $n_{\text{ex}}(x)$ | $\bar{n} + \Delta n_l/2$ | $\bar{n} + (\Delta n_l/2)\cos(2x\pi/\Lambda)$ |
| $n_{\text{or}}(x)$ | $\bar{n} - \Delta n_l/2$ | $\bar{n} - (\Delta n_l/2)\cos(2x\pi/\Lambda)$ |
| $G(x)$ | 0 | $\bar{n}\Delta n_c \sin(2x\pi/\Lambda)$ |

$$\tilde{\epsilon}_{\text{cir}} = \begin{bmatrix} 0 & -iG & 0 \\ iG & 0 & 0 \\ 0 & 0 & 0 \end{bmatrix}, \quad (2b)$$

where $n_{\text{or}}(x)$ and $n_{\text{ex}}(x)$ are the refractive indices observed by linearly polarized light in the ordinary (perpendicular) and extraordinary (parallel) directions of the uniaxial anisotropy (linear birefringence is defined as $\Delta n_l = n_{\text{ex}} - n_{\text{or}}$). The gyration factor $G(x) = \bar{n}\Delta n_c$ is symmetric about the z axis [where $\bar{n} = \frac{1}{2}(n_{\text{or}} + n_{\text{ex}})$ is the average index of refraction and the circular birefringence is identified as Δn_c]. \mathbf{R} is a rotation matrix where $\phi(x)$ is the azimuth angle measured from the x axis as follows:

$$\mathbf{R}(\phi) = \begin{bmatrix} \cos(\phi) & -\sin(\phi) & 0 \\ \sin(\phi) & \cos(\phi) & 0 \\ 0 & 0 & 1 \end{bmatrix}. \quad (3)$$

The profiles of the two PG types (circular and linear) can now be fully defined by their anisotropy profile (ϕ , n_{or} , n_{ex} , and G) in terms of material parameters (\bar{n} , Δn_l , and Δn_c) and geometry (thickness d and effective optical period Λ). These are defined in Table I and Fig. 2.

The diffraction angle θ_m of the m -order propagating wave [Fig. 2(c)] is determined by the grating equation

$$\sin \theta_m = m\lambda/\Lambda + \sin \theta_{\text{inc}}, \quad (4)$$

where θ_{inc} is the angle of incidence. The complex vector amplitude \mathbf{E}_m in the far field of the m -order propagating wave is calculated by a (Fourier) vector transformation applied to a line sampled immediately following the structure [defined explicitly in Eqs. (18) in Ref. [22]].

Except where noted (Sec. III C), diffraction efficiencies are calculated as the ratio of the intensity of wave m to the total intensity of the forward propagating waves as follows:

$$\eta_m = |\mathbf{E}_m|^2 / |\mathbf{E}_{\text{tot}}|^2, \quad (5)$$

where $|\mathbf{E}_{\text{tot}}|^2 = \sum_{m=-\infty}^{+\infty} |\mathbf{E}_m|^2$.

To appropriately isolate the effect of the PGs themselves from Fresnel reflection effects, we place gradient-index anti-reflection layers [28] at the air-PG interfaces. The computational grid spacing was selected as $\Delta u = \lambda_{\text{min}}/20n_{\text{max}}$, where λ_{min} is the shortest wavelength of interest and n_{max} is the maximum index of refraction in the media. The time resolution was chosen as $\Delta t = \Delta u/3c$ to ensure numerical stability, where c is the speed of light. Except where noted, the expected accuracy of the FDTD simulation is $\approx 0.05\%$ (mean-square error).

III. FDTD ANALYSIS OF CIRCULAR PGs

A set of analytic expressions for the diffraction efficiency of an infinite circular PG have been derived using Jones calculus for normally incident light [18] (a reformulation of Refs. [1,3]) as follows:

$$\eta_0 = \cos^2(\pi\Delta n_l d/\lambda), \quad (6a)$$

$$\eta_{\pm 1} = \frac{1 \mp S'_3}{2} \sin^2(\pi\Delta n_l d/\lambda), \quad (6b)$$

where λ is the wavelength, η_m is the diffraction efficiency of the m order, Δn_l is the linear birefringence, d is the grating thickness, and $S'_3 = S_3/S_0$ is the normalized Stokes parameter [29] of the input light. Furthermore, it can be shown that the polarization states of the ± 1 orders will be orthogonal and circularly polarized (hence the label ‘‘circular PG’’).

The expressions above are derived using the paraxial approximation (that all waves of interest propagate along directions close to the z axis), which necessarily implies that the gratings are considered ‘‘thin.’’ Several unique features are apparent: only three orders are potentially nonzero ($\eta_{|m|\geq 2} = 0$, unlike thin phase gratings); all three orders can have efficiencies from 100% to 0%; both η_0 and the sum of $\eta_{\pm 1}$ depend only on the normalized retardation $\Delta n_l d/\lambda$; and each of the ± 1 -order efficiencies varies strongly with the input polarization.

We begin our FDTD analysis with a comparison to Eqs. (6), and subsequently proceed by examining off-axis illumination, considering the limits of the thin-grating regime (well beyond paraxial), and predicting the behavior of a finite grating.

A. Fundamental diffraction properties

The numerically calculated diffraction efficiencies of a circular PG are shown in Fig. 3(a), compared to the analytic prediction from Eq. (6). The grating parameters were $\Lambda = 20\lambda_0$, $d = 5\lambda_0$, $\bar{n} = 1.6$, and $\Delta n_l = 0.2$, where λ_0 is the center wavelength of the input source and the numerical wavelength of the simulation. We used a Gaussian-pulsed plane wave [22] with linear, vertical polarization as the input. As expected, only three diffraction orders (0, ± 1) are nonzero ($>0.01\%$), and the maximum first-order efficiency approaches 100% (actually 99.96%). We note that the maximum efficiency is influenced by the grating parameters (e.g., Λ/λ), which will be discussed in Sec. III B. We also verified the polarization states of each diffraction order; the zero order has the same linear polarization state as the input and the +1 and -1 orders have right- and left-hand circular polarizations.

The polarization sensitivity of the first orders is shown in Fig. 3(b), which plots the calculated diffraction for different ellipticity angles [29] of the incident polarization when $\Delta n_l d = \lambda/2$ (i.e., when $\eta_0 \approx 0$). The ellipticity angle χ is related to the normalized Stokes parameter by $S'_3 = \sin(2\chi)$. The FDTD field maps, captured using a monochromatic source, are presented in Fig. 4, for circular ($\chi = \pi/4$) and linear ($\chi = 0$) incident polarizations. Animated movies of these two

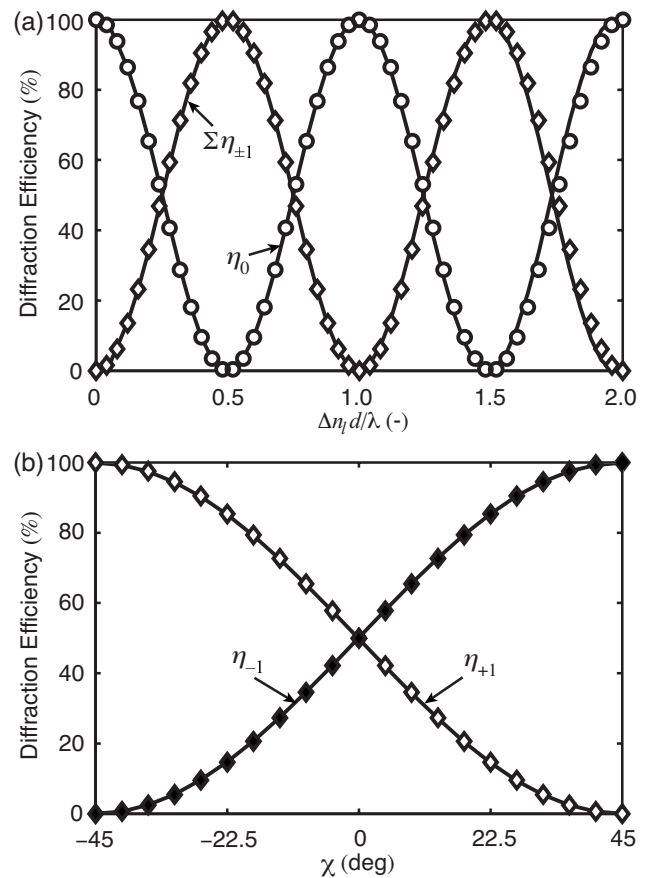


FIG. 3. Diffraction behavior of a circular PG—(a) diffraction efficiency spectra and (b) polarization-sensitive first-order diffraction ($\Delta n_l d/\lambda = 1/2$)—numerically calculated (curves) and analytically estimated (\circ , \diamond , and \blacklozenge) using Eqs. (6), where $\Delta n_l d/\lambda$ is the normalized retardation and χ is the ellipticity angle of the incident polarization. ($\Lambda = 20\lambda_0$, $\bar{n} = 1.6$, $\Delta n_l = 0.2$.)

cases are available at EPAPS Ref. [30]. Overall, the FDTD calculation correlates extremely well to the analytic expressions of Eq. (6).

The angular response is shown in Fig. 5, where the impact of oblique illumination is highlighted (a topic not yet theoretically studied, to our knowledge). The grating parameters were $\Lambda = 20\lambda_0$, $d = 5\lambda_0$, $\bar{n} = 1.6$, and $\Delta n_l = 0.2$. The Gaussian pulse was again used as the source, with right-handed circular polarization input. For small angles of incidence θ_{inc} , only the -1 order has appreciable power ($\approx 100\%$) and manifests a nearly perfect right-handed circular polarization ($S'_3 \approx 1$). For $|\theta_{\text{inc}}| > 20^\circ$, the -1-order efficiency decreases (with the leakage passing into the zero order), and its polarization state becomes increasingly elliptical. Note that the angular response is asymmetric with respect to $\theta_{\text{inc}} = 0$. We consider all of these off-axis effects as being primarily related to a change in the effective optical path length experienced by the incident lightwave as θ_{inc} increases.

B. Beyond the paraxial approximation

While excellent agreement is observed between the FDTD results and analytical solutions for the paraxial case,

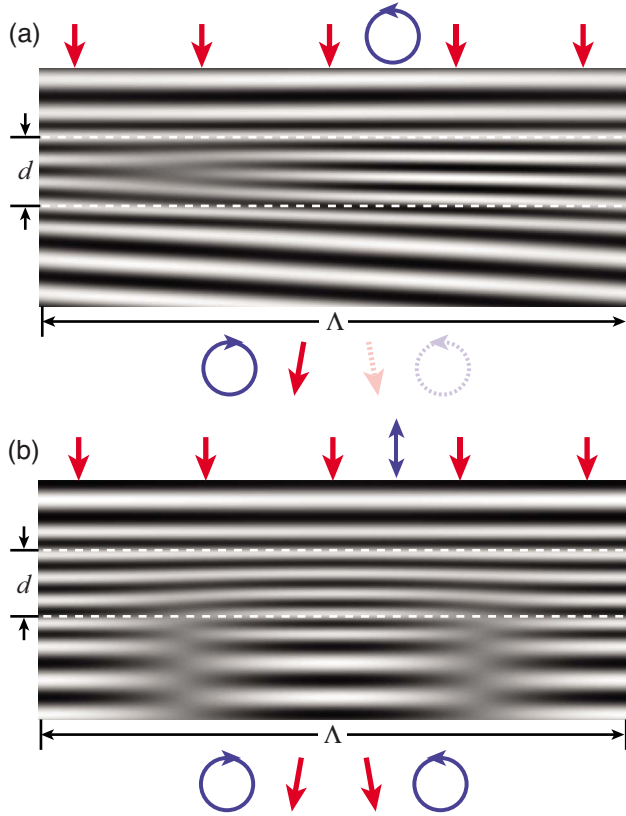


FIG. 4. (Color online) FDTD near-field images of wave propagation through a circular PG for (a) right-handed circular ($\chi=\pi/4$) and (b) vertical linear ($\chi=0$) incident polarization, with WOLFSIM. Animated movies are available at EPAPS Ref. [30]. ($\Lambda=20\lambda$, $\bar{n}=1.6$, $\Delta n_l=0.2$, $d=\lambda/2\Delta n_l$.)

the small-angle assumptions used in the derivation of Eqs. (6) suggest that they may not describe diffraction if Λ/λ is not large. Several fundamental questions therefore remain unanswered: For what PG parameters do the analytic equations apply? Is the Klein parameter Q [31,32] useful to distinguish grating regimes in PGs, or is another parameter more descriptive? For a given λ and Λ , what choice of d , Δn_l , and \bar{n} enables high efficiencies?

The best way to address these questions is to consider a parameter space defined by the normalized retardation $\Delta n_l d/\lambda$ and grating period Λ/λ_0 (similar to Ref. [33] for phase gratings). This is essentially a summary of diffraction spectra versus grating period. In Fig. 6, we present a map of the total first-order diffraction for a relatively high ($\Delta n_l=0.2$) and low ($\Delta n_l=0.04$) birefringence. We plot the FDTD result as solid-line contours, and plot the analytic expressions [Eqs. (6)] as grayscale levels. Note that these are well correlated for larger values of Λ/λ_0 , but become dramatically different for smaller grating periods. The FDTD calculation was generated as follows: for each setting of Λ/λ_0 , a Gaussian-pulsed plane wave [22] was input with linear, vertical polarization, and the normalized spectral output ($\sum \eta_{\pm 1}$ versus $\Delta n_l d/\lambda$) was calculated. Additionally, $d=\lambda_0/2\Delta n_l$ and $\bar{n}=1.6$.

It is instructive to segment this first-order efficiency map into grating regimes, often described as either *thin* or *thick*.

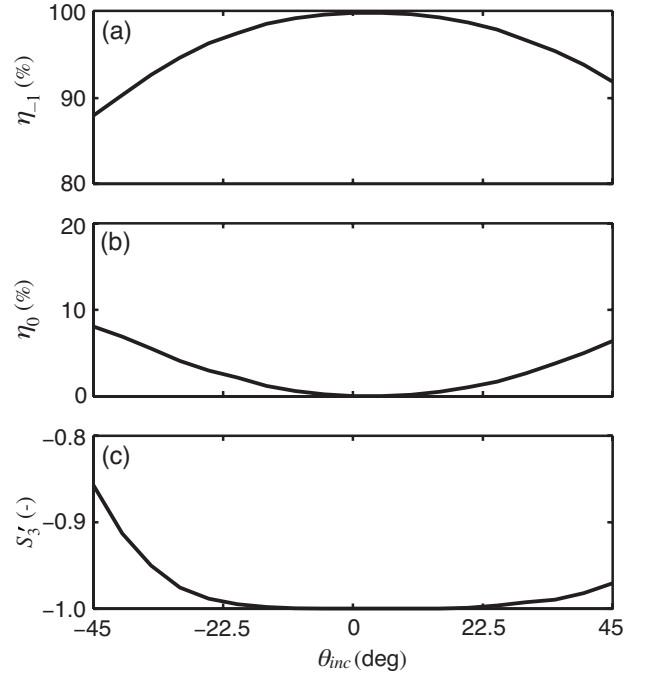


FIG. 5. Angular response of a circular PG when illuminated at oblique incidence with right-handed circular polarization input ($\chi=45^\circ$): (a) First-order and (b) zero-order diffraction efficiency; (c) polarization state of the diffracted -1 order. PG parameters are set for half-wave retardation. ($\Lambda=20\lambda$, $d=5\lambda$, $\bar{n}=1.6$, and $\Delta n_l=0.2$.)

In classical grating analysis, two dimensionless parameters Q [31,32] and ρ [34] are frequently used to identify the grating regimes as follows:

$$Q = \frac{2\pi\lambda d}{\bar{n}\Lambda^2}, \quad (7)$$

$$\rho = \frac{2\lambda^2}{\bar{n}\Delta n_l\Lambda^2}. \quad (8)$$

We make the conjecture that $\Delta n_l=2n_1$, where n_1 is the index modulation amplitude of coupled-wave theory.

The contours of both parameters are superimposed on the map in Fig. 6. The condition $Q < 1$ is most popularly used to identify the thin-grating (Raman-Nath) regime, and it is appropriate to note that the analytic equations [Eqs. (6)] correspond well to the FDTD solution under this same condition. However, it is important to note that this is sufficient, but not necessary: for some regions with $Q > 1$, it is still possible for the FDTD solution to be nearly identical to the analytic solutions (especially for larger values of $\Delta n_l d/\lambda$). This suggests that Q is not the best indicator of the thin-grating regime boundary. In fact, this is generally true for phase gratings [34], but is particularly noticeable in circular PGs since their birefringence can be high.

A contour for the parameter $\rho=1$ is also shown in Fig. 6. Note that because the FDTD and analytic solutions correlate strongly when $\rho < 1$, this parameter [Eq. (8)] is the most robust indication of when Eqs. (6) are valid. The usefulness

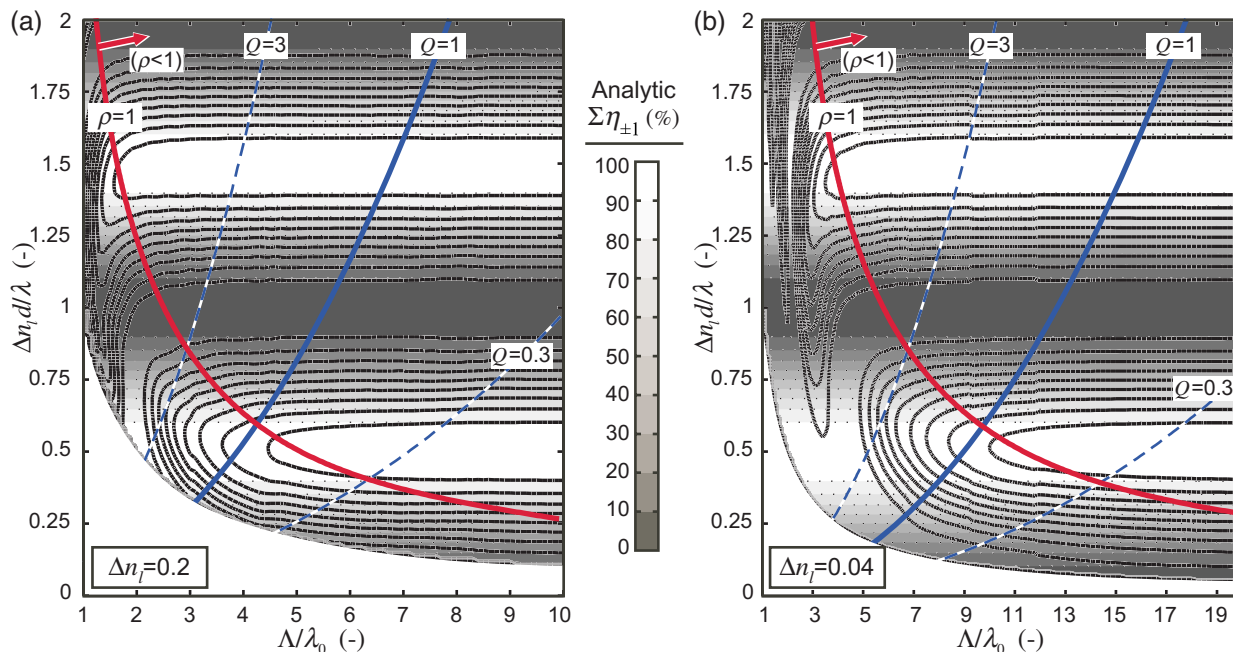


FIG. 6. (Color online) The behavior of circular PG diffraction with respect to grating regime (thin or thick), from the perspective of Q and ρ parameters [31,32,34]. The contour plots show the total first-order diffraction $\Sigma\eta_{\pm 1}$ versus normalized retardation $\Delta n_l d/\lambda$ and normalized grating period Λ/λ_0 . A comparison between numerical FDTD calculation (black solid-line contours) and analytical estimate (grayscale levels) is shown for a high ($\Delta n_l=0.2$) and low ($\Delta n_l=0.04$) birefringence in parts (a) and (b), respectively. We note that diffraction best follows the analytic expressions [Eqs. (6)] when $\rho < 1$, the thin-grating regime. The input wave is normally incident, and the crosshatch indicates $\lambda/\Lambda > 1$, when the first-order diffraction modes become evanescent.

of ρ over Q is particularly important when large diffraction angles are desired (i.e., Λ/λ approaching 1). Assuming normally incident light, we therefore predict that the following conditions must be met for $\approx 100\%$ diffraction in circular PGs: $\rho < 1$ and $\Delta n_l d/\lambda = 1/2 + a$, where a is a non-negative integer.

A complementary view of circular PG behavior is shown in Fig. 7. A series of FDTD simulations were performed with a normally incident, linearly polarized, Gaussian-pulsed plane-wave input for a range of Λ and Δn_l . The first maximum of the first-order diffraction efficiency $\Sigma\eta_{\pm 1, \max}$ (which appears at or near the $\Delta n_l d/\lambda = 1/2$ line in Fig. 6) decreases as Λ approaches λ . We normalize with respect to the actual wavelength λ_{\max} at which each maximum occurs. One apparent lesson about circular PGs is therefore that materials that possess a high linear birefringence are needed in order to achieve high diffraction efficiencies and large diffraction angles.

The discussion in this subsection has assumed that $\theta_{\text{inc}} = 0^\circ$. While it would indeed be interesting to study the diffraction in thick circular PGs ($\rho > 1$) with oblique illumination, it remains outside the scope of this work.

C. Finite grating effects

In many application contexts (most notably in displays [35,36]), finite-size PGs are inherently involved because the transverse direction of the grating is bounded in some way (e.g., by pixel edges). It is therefore important to quantify the diffraction of this finite grating as its lateral size L becomes

comparable to the grating period Λ . To accomplish this, we have created a pixel model by surrounding a circular PG in the lateral direction by UPML absorbing media. Additionally, all four boundaries of the simulation space are terminated by UPML boundaries.

The near-field and far-field diffraction of an example pixel ($L=2\Lambda$) with a circular PG ($\Lambda=10\lambda$, $\Delta n_l d=\lambda/2$, and $\bar{n}=1.6$) and an isotropic dielectric slab are shown in Figs. 8(a) and 8(b). A monochromatic plane wave with right-hand cir-

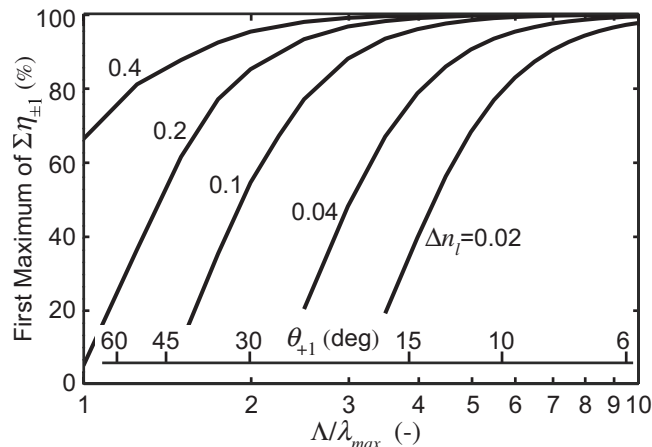


FIG. 7. The first maximum of the first-order diffraction $\Sigma\eta_{\pm 1}$ of the circular PG (calculated numerically). The normalization factor λ_{\max} is the wavelength at which maximum diffraction occurs. Note that the axis for $\theta_{\pm 1}$ shows the angle of diffraction for the given ratio Λ/λ_{\max} .

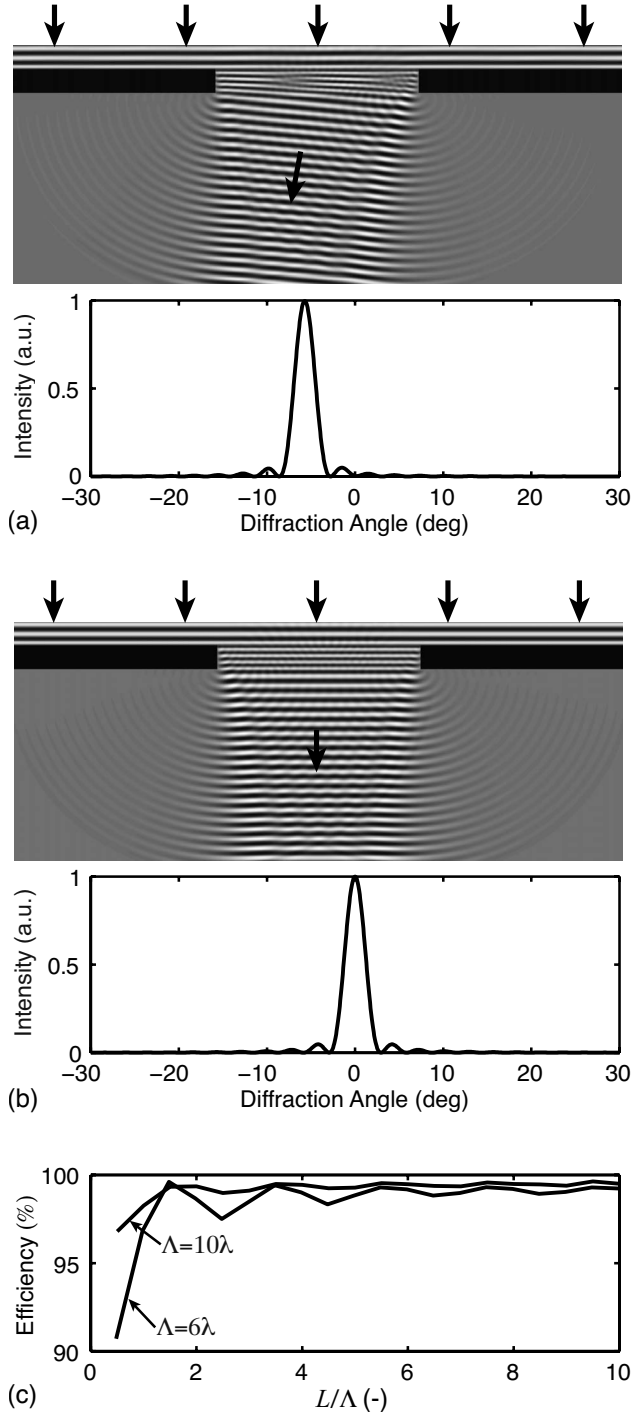


FIG. 8. Diffraction behavior of finite circular PGs. We show the near-field images and intensity profiles of (a) a finite circular PG and (b) a dielectric slab, when $L=2\Lambda$ and $\Lambda=10\lambda$. In part (c), the first-order efficiencies of two finite circular PGs with $\Lambda=6\lambda$ and 10λ are compared for various pixel sizes up to $L=10\Lambda$ for each case. Animated movies of the fields are available (Ref. [30]). ($\bar{n}=1.6$, $\Delta n_l=0.2$, and $d=\lambda/2\Delta n_l$.)

cular polarization was input with normal incidence, and the far-field intensity calculated with the standard Kirchhoff integral method for finite apertures (e.g., Ref. [37]). Since the far-field intensity profiles follow the classical single-slit aperture diffraction ($I(\theta) \propto \text{sinc}^2[\pi \sin(\theta - \theta_m)L/\lambda]$, with θ_m

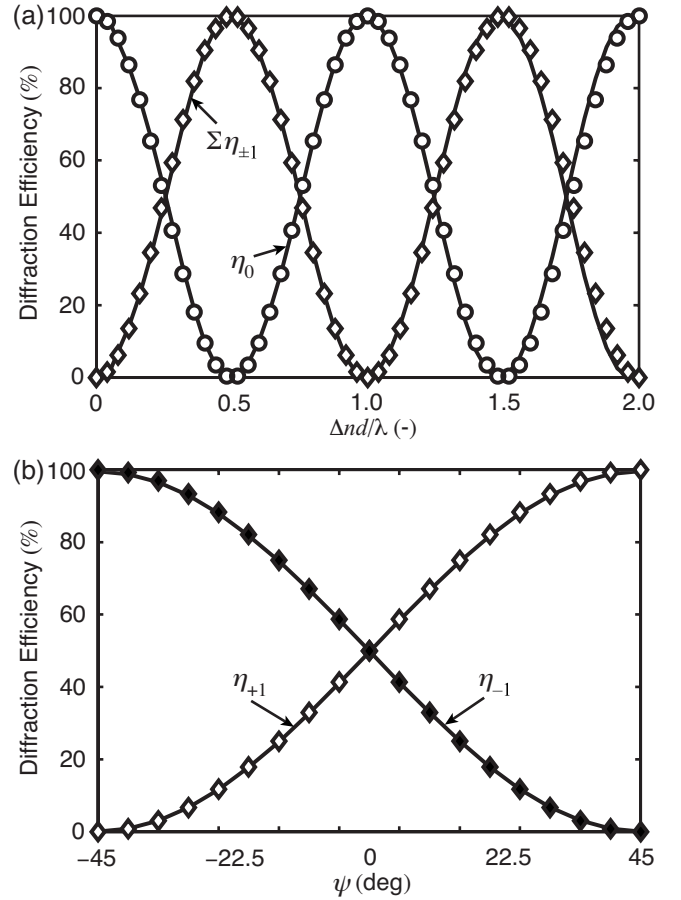


FIG. 9. Diffraction behavior of a linear PG ($\Delta n_l = \Delta n_c = \Delta n = 0.2$)—(a) diffraction efficiency spectra and (b) polarization-sensitive first-order diffraction ($\Delta nd/\lambda = 1/2$)—numerically calculated (curves) and analytically estimated (\circ , \diamond , and \blacklozenge) using Eqs. (10). ($\Lambda = 20\lambda_0$, $\bar{n} = 1.6$.)

$= 0$ for the dielectric slab), the diffraction efficiency is no longer strictly a scalar. However, we can still make useful comparisons between the two cases of Fig. 8 by defining the diffraction efficiency for finite PGs as

$$\eta = \frac{(I_{\text{peak}}/I_{\text{tot}})_{\text{PG}}}{(I_{\text{peak}}/I_{\text{tot}})_{\text{SLAB}}}, \quad (9)$$

where I_{peak} and I_{tot} are the maximum and total intensities in the far field in the two simulations. In this way, we isolate the diffraction effect of the grating as opposed to the aperture.

Figure 8(c) shows the -1 -order efficiency when $\Lambda = 10\lambda$ and 6λ . As might be expected, we observe that as L/Λ increases, the efficiency asymptotically approaches the value (99.5%) of the comparable infinite PG. Furthermore, a weak oscillation away from this maximal value becomes increasingly pronounced for smaller grating periods (Λ/λ). However, this analysis suggests that a high efficiency can still be achieved even with a small pixel size (e.g., $L \approx 12 \mu\text{m}$, for $\lambda = 550 \text{ nm}$ and $\Lambda = 3.3 \mu\text{m}$).

IV. FDTD ANALYSIS OF LINEAR PGs

Linear PGs are distinct from circular PGs because they have a periodic modulation in the magnitude of their linear

and circular birefringences [Fig. 1(b)], attainable in various materials [1,7,12,38]. Classification into two cases is convenient: (a) $\Delta n_l = \Delta n_c$ and (b) $\Delta n_l \neq \Delta n_c$.

A. Linear PGs with $\Delta n_c = \Delta n_l$

The presence of the circular birefringence (Δn_c) makes the diffraction properties of linear PGs distinct. When $\Delta n_l = \Delta n_c$, interesting diffraction properties result: again only three diffracted orders are present, but the first-order beams are linearly polarized and their efficiencies are strongly dependent on the extent of linear polarization present in the incident light. Analytic expressions can be derived using Jones calculus (a reformulation of Ref. [7]) under the same assumptions as before as follows:

$$\eta_0 = \cos^2(\pi\Delta nd/\lambda), \quad (10a)$$

$$\eta_{\pm 1} = \frac{1 \mp S'_1}{2} \sin^2(\pi\Delta nd/\lambda), \quad (10b)$$

where $\Delta n = \Delta n_l = \Delta n_c$ and $S'_1 = S_1/S_0$ is the normalized Stokes parameter [29] of the input light. Since the polarization states of the ± 1 orders will be orthogonal and linearly polarized, the label “linear PG” applies.

The numerical and analytic diffraction spectra of linear PGs correspond well, and are shown in Fig. 9(a), with $\Lambda = 20\lambda_0$, $d = 5\lambda_0$, $\bar{n} = 1.6$, and $\Delta n = 0.2$. As expected, only three diffraction orders are present, and the maximum first-order efficiency approaches 100% (actually, 99.73%). We also verified the polarization states of each diffraction order; the zero order has the same polarization state as the input and the +1 and -1 orders have horizontal and vertical linear polarizations. We also examined the paraxial limit for the ideal diffraction of the linear PG, in the same manner as Sec. III B and Fig. 6. The resulting behavior of the linear PG was the same as for the circular PG with respect to the grating regime and conditions for high diffraction efficiency, and the discussion in that section (Sec. III B) therefore also applies to linear PGs. Note that we omit the figures for linear PGs because they appear identical.

The polarization sensitivity is shown in Fig. 9(b) with respect to the orientation angle [29] of the linearly polarized incident light [$S'_1 = \cos(2\psi)$]. We emphasize that the first-diffraction orders of linear PGs respond to the orientation and extent of *linear polarization* in the incident light, while circular PGs respond to the ellipticity and extent of *circular polarization*. The FDTD near-field maps of linear PG with a monochromatic source appear identical to Figs. 4(a) and 4(b) for vertical linear incident polarization and right-handed circular incident polarization, respectively, and are therefore omitted.

B. Linear PGs with $\Delta n_c \neq \Delta n_l$

Unlike the two previous PGs examined so far, linear PGs with $\Delta n_c \neq \Delta n_l$ exhibit nonzero higher diffraction orders ($\eta_{|m| \geq 2} \neq 0$), similar to thin phase and amplitude gratings. However, diffraction properties depend strongly [7] on the birefringence ratio $\Delta n_c/\Delta n_l$, and we can identify several in-

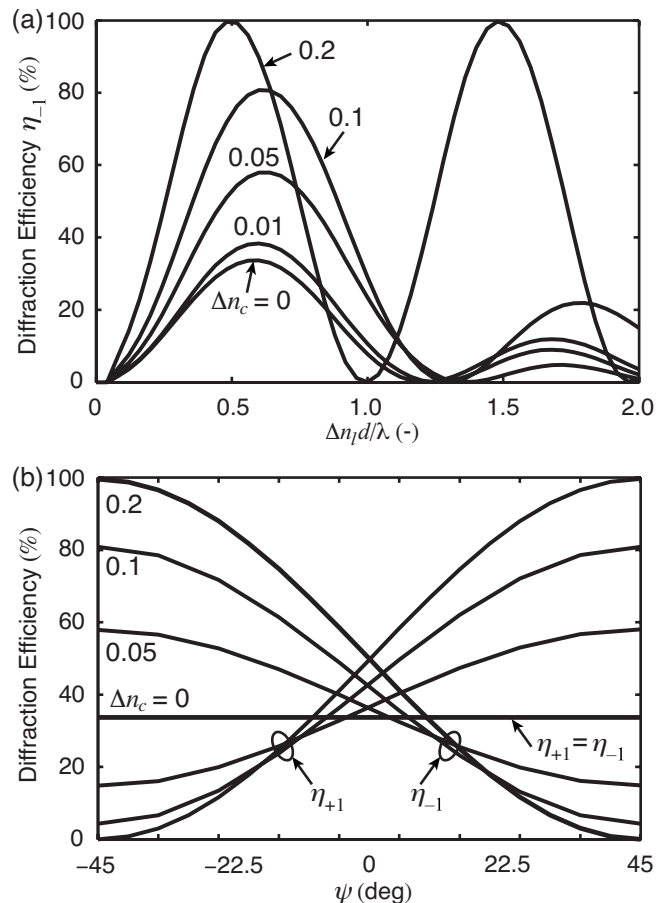


FIG. 10. Diffraction behavior of the linear PG ($\Delta n_c \neq \Delta n_l$) for different values of circular birefringence Δn_c : (a) diffraction efficiency spectra and (b) polarization-sensitive first-order diffraction ($\Delta n_l/\lambda = 1/2$). ($\Lambda = 20\lambda$, $d = 5\lambda$, $\bar{n} = 1.6$, and $\Delta n_l = 0.2$.)

teresting cases: for $\Delta n_c = 0$, light diffracted into odd orders of linear PGs alter the incident light as if traveling through a $\lambda/2$ wave plate whose fast axis is at 45° ; for $\Delta n_l = 0$, the odd orders act as a 90° polarization rotator. In both of these extremes, the diffraction efficiencies follow $\eta_m = J_m^2(\pi\Delta nd/\lambda)$.

Diffraction spectra for various $\Delta n_c/\Delta n_l$ ratios with linearly polarized input are shown in Fig. 10(a), where $\Delta n_l = 0.2$, $\Lambda = 20\lambda_0$, $d = 5\lambda_0$, and $\bar{n} = 1.6$. When $\Delta n_c = 0$, it should be noted that only the magnitude (and not the orientation) of its linear birefringence is varying spatially, and as such, these linear PGs show very similar diffraction behaviors to conventional phase gratings: multiple diffraction orders and no polarization sensitivity. However, as Δn_c increases, the maximum diffraction efficiency increases, and the first orders become sensitive to the incident polarization (i.e., $\propto S'_1$). Both of these effects can be observed [Fig. 10(b)] in the polarization contrast between the $m = \pm 1$ orders. It is important to note the local influence that a linear PG imposes on incident light: the linear birefringence locally modifies the polarization orientation, while simultaneously the circular birefringence modifies its ellipticity—both in a spatially dependent fashion. When the variation in the two types of anisotropy is balanced, linear PGs manifest properties in response to linear incident polarizations, which are analogous to circular PGs illuminated with circular polarizations.

V. CONCLUSION

This work is the first general numerical analysis of the primary types of PGs (circular and linear), and presents their diffraction behavior on a fundamental level with as few assumptions as possible. Using our newly developed FDTD method for periodic anisotropic media, we found strong correspondence with the analytic expressions previously developed for “thin” PGs (i.e., with small diffraction angles and normally incident illumination). A fundamental view at polarized wave behavior within PGs is presented using electric-field maps and animations. We explored the thin-thick grating regime transition, and identified $\rho < 1$ as the most robust condition (as opposed to $Q < 1$) to delineate the grating regime. It is also apparent that materials with large linear birefringence are most likely to support a high diffraction efficiency and large diffraction angle simultaneously. In

studying off-axis illumination, we found that PGs can retain high diffraction efficiencies for modest incident angles ($< 20^\circ$). We also studied the behavior of a finite grating, and found that first-order diffraction remains nearly identical in magnitude to that of a comparably small aperture (i.e., high diffraction efficiency occurs even for only a few grating periods). The numerical analysis techniques employed here have been integrated into our open-source FDTD software package (WOLFSIM), which is freely available on the Web [23].

ACKNOWLEDGMENTS

The authors gratefully acknowledge support from the National Science Foundation (Grants No. ECCS-0621906 and No. IIP-0539552), ImagineOptix Inc., and Southeast TechInventures Inc.

-
- [1] L. Nikolova and T. Todorov, *Opt. Acta* **31**, 579 (1984).
 [2] T. Huang and K. Wagner, *IEEE J. Quantum Electron.* **31**, 372 (1995).
 [3] F. Gori, *Opt. Lett.* **24**, 584 (1999).
 [4] J. Tervo and J. Turunen, *Opt. Lett.* **25**, 785 (2000).
 [5] E. Hasman, Z. Bomzon, A. Niv, G. Biener, and V. Kleiner, *Opt. Commun.* **209**, 45 (2002).
 [6] G. Cincotti, *IEEE J. Quantum Electron.* **39**, 1645 (2003).
 [7] L. Nikolova, T. Todorov, M. Ivanov, F. Andruzzi, S. Hvilsted, and P. S. Ramanujam, *Appl. Opt.* **35**, 3835 (1996).
 [8] N. Holme, L. Nikolova, P. Ramanujam, and S. Hvilsted, *Appl. Phys. Lett.* **70**, 1518 (1997).
 [9] G. Martinez-Ponce, T. Petrova, N. Tomova, V. Dragostinova, T. Todorov, and L. Nikolova, *J. Opt. A, Pure Appl. Opt.* **6**, 324 (2004).
 [10] S. Slussarenko, O. Francescangeli, F. Simoni, and Y. Reznikov, *Appl. Phys. Lett.* **71**, 3613 (1997).
 [11] Y. Okada-Shudo, *Proc. SPIE* **4461**, 138 (2001).
 [12] H. Ono and A. Emoto, *Opt. Express* **11**, 2379 (2003).
 [13] J. A. Davis, J. Adachi, C. R. Fernandez-Pousa, and I. Moreno, *Opt. Lett.* **26**, 587 (2001).
 [14] B. Wen, R. G. Petschek, and C. Rosenblatt, *Appl. Opt.* **41**, 1246 (2002).
 [15] G. P. Crawford, J. N. Eakin, M. D. Radcliffe, A. Callan-Jones, and R. A. Pelcovits, *Appl. Phys. Lett.* **85**, 1671 (2004).
 [16] H. Sarkissian, S. V. Serak, N. V. Tabiryan, L. B. Glebov, V. Rotar, and B. Y. Zeldovich, *Opt. Lett.* **31**, 2248 (2006).
 [17] M. J. Escuti and W. M. Jones, *SID Int. Symp. Digest Tech. Papers* **37**, 1443 (2006).
 [18] M. J. Escuti, C. Oh, C. Sanchez, C. W. M. Bastiaansen, and D. J. Broer, *Proc. SPIE* **6302**, 632614 (2006).
 [19] C. Provenzano, P. Pagliusi, and G. Cipparrone, *Appl. Phys. Lett.* **89**, 121105 (2006).
 [20] A. Taflove and S. C. Hagness, *Computational Electrodynamics: Finite-Difference Time-Domain Method*, 2nd ed. (Artech House, Norwood, MA, 2000).
 [21] R. C. Jones, *J. Opt. Soc. Am.* **31**, 488 (1941).
 [22] C. Oh and M. J. Escuti, *Opt. Express* **24**, 11870 (2006).
 [23] <http://www.ece.ncsu.edu/oleg/wolfsim.html>
 [24] K. S. Yee, *IEEE Trans. Antennas Propag.* **14**, 302 (1966).
 [25] J. A. Roden, S. D. Gedney, M. P. Kesler, J. G. Maloney, and P. H. Harms, *IEEE Trans. Microwave Theory Tech.* **46**, 420 (1998).
 [26] S. D. Gedney, *IEEE Trans. Antennas Propag.* **44**, 1630 (1996).
 [27] G. R. Fowles, *Introduction to Modern Optics* (Holt, Rinehart and Winston, New York, 1968).
 [28] W. H. Southwell, *Opt. Lett.* **8**, 584 (1983).
 [29] E. Collett, *Polarized Light: Fundamentals and Applications* (Dekker, New York, 1993).
 [30] See EPAPS Document No. E-PLRAAN-76-116707 for animations of wave propagation in circular PGs. For more information on EPAPS, see <http://www.aip.org/pubservs/epaps.html>. Also available at <http://www.ece.ncsu.edu/oleg/PolarizationGratings>
 [31] W. R. Klien and B. D. Cook, *IEEE Trans. Sonics Ultrason.* **14**, 123 (1967).
 [32] H. Kogelnik, *Bell Syst. Tech. J.* **48**, 2909 (1969).
 [33] I. Richter, Z. Ryzi, and P. Fiala, *J. Mod. Opt.* **16**, 1915 (1991).
 [34] M. G. Moharam and L. Yong, *Appl. Opt.* **17**, 1757 (1978).
 [35] W. M. Jones, B. L. Conover, and M. J. Escuti, *SID Int. Symp. Digest Tech. Papers* **37**, 1015 (2006).
 [36] R. K. Komanduri, W. M. Jones, C. Oh, and M. J. Escuti, *Journal of the SID* **15**, 589 (2007).
 [37] M. Born and E. Wolf, *Principles of Optics*, 7th ed. (Cambridge University Press, New York, 1999).
 [38] I. Naydenova, L. Nikolova, T. Todorov, F. Andruzzi, S. Hvilsted, and P. Ramanujam, *J. Mod. Opt.* **44**, 1643 (1997).